Structural basis of human γ-secretase assembly

Linfeng Sun[1], Lingyun Zhao[1], Guanghui Yang[1], Chuangye Yan[1], Rui Zhou[1], Xiaoyuan Zhou, Tian Xie, Yanyu Zhao, Shenjie Wu, Xueming Li, and Yigong Shi (施一公)[2]

Ministry of Education Key Laboratory of Protein Science, Tsinghua–Peking Joint Center for Life Sciences, Center for Structural Biology, School of Life Sciences, Tsinghua University, Beijing 100084, China

Contributed by Yigong Shi, April 2, 2015 (sent for review March 16, 2015; reviewed by Huilin Li and Gang Yu)

The four-component intramembrane protease γ-secretase is intricately linked to the development of Alzheimer's disease. Despite recent structural advances, the transmembrane segments (TMs) of γ-secretase remain to be specifically assigned. Here we report a 3D structure of human γ-secretase at 4.32-Å resolution, determined by single-particle, electron cryomicroscopy in the presence of digitonin and with a T4 lysozyme fused to the amino terminus of presenilin 1 (PS1). The overall structure of this human γ-secretase is very similar to that of wild-type γ-secretase determined in the presence of amphipols. The 20 TMs are unambiguously assigned to the four components, revealing principles of subunit assembly. Within the transmembrane region, PS1 is centrally located, with its amino-terminal fragment (NTF) packing against Pen-2 and its carboxyl-terminal fragment (CTF) interacting with Aph-1. The only TM of nicastrin associates with Aph-1 at the thick end of the TM horseshoe, and the extracellular domain of nicastrin directly binds Pen-2 at the thin end. TM6 and TM7 in PS1, which harbor the catalytic aspartate residues, are located on the convex side of the TM horseshoe. This structure serves as an important framework for understanding the function and mechanism of γ-secretase.

γ-secretase | cryo-EM structure | Presenilin | intramembrane protease | Alzheimer's disease

Alzheimer's disease (AD), characterized by formation of β-amyloid plaque in the brain of a patient, is closely associated with γ-secretase (1, 2). Amyloid precursor protein (APP) is processed by β-secretase in the extracellular space to produce a membrane-tethered fragment known as C99 (3). APP C99 then undergoes sequential cleavages by γ-secretase, generating a series of β-amyloid peptides (Aβ) exemplified by Aβ42 and Aβ40 (4, 5). Among all Aβs, Aβ42 is particularly prone to aggregation, resulting in formation of β-amyloid plaque and presumably contributing to the development of AD (6).

Mature γ-secretase contains four components: presenilin, Pen-2, nicastrin, and Aph-1. The catalytic subunit presenilin is predicted to contain nine transmembrane segments (TMs), with two catalytic aspartate residues on TM6 and TM7. During assembly of γ-secretase, presenilin undergoes an autocatalytic cleavage to yield two polypeptide fragments, NTF (comprising TMs 1–6) and CTF (comprising TMs 7–9) (7, 8). PS1 is the target of most mutations derived from early onset familial Alzheimer's disease patients (1). The largest component nicastrin has only one TM but contains a highly glycosylated extracellular domain (ECD), which presumably recognizes the amino terminus of substrate protein (9–11). The smallest component Pen-2 is thought to be required for the autocatalytic maturation of presenilin and γ-secretase activity (12, 13). Aph-1, required for assembly of γ-secretase (14), appears to have a previously unidentified fold with seven predicted TMs.

The assembly and intersubunit interactions of γ-secretase constitute an important basis for its mechanistic understanding and have been extensively investigated during the past decade. As the central component of γ-secretase, PS1 was shown to interact with both Pen-2 and Aph-1 and form distinct subcomplexes (15–21). The only TM of nicastrin was thought to bind Aph-1 and contribute to interactions with PS1. Rationalization of these biochemical findings and other functional observations requires detailed 3D structural information on γ-secretase.

In contrast to rapid accumulation of biochemical and functional data on γ-secretase, structural determination has been slow to emerge, largely due to the technical challenges associated with expression and manipulation of the intact γ-secretase. Several EM analyses have yielded low-resolution images of γ-secretase (22–27), with the overall shapes diverging from each other. Investigation of γ-secretase by other biophysical methods produced an NMR structure of the presenilin CTF (28) and X-ray structures of an archaeal homolog of presenilin (29) and a eukaryotic homolog of nicastrin (30).

The high-resolution cryo-electron microscopy (cryo-EM) structure of human γ-secretase, determined at 4.5-Å resolution and in the presence of amphipols, revealed an overall architecture that is qualitatively different from all previous structures (31). The EM densities allowed identification of 19 TMs and construction of an atomic model for the ECD (31). However, these densities lacked connectivity between TMs and exhibited few side-chain features in the TMs, disallowing specific TM assignment to the four components. The use of amphipols also raises the question of whether the structure of human γ-secretase is dependent upon the choice of detergent used. In this study, we address these concerns and report, to our knowledge, the first structure of an intact γ-secretase with all TMs assigned.

Significance

Unlike other single-component intramembrane proteases such as rhomboid and S2P, γ-secretase contains four components: presenilin, Pen-2, Aph-1, and nicastrin. Previous electron cryomicroscopy (cryo-EM) analysis of human γ-secretase in amphipols revealed its overall architecture and 19 distinct transmembrane segments (TMs). However, the lack of side-chain density in the TMs, together with disordered inter-TM loops, disallowed TM assignment. Our current cryo-EM structure of human γ-secretase at 4.32-Å resolution allows specific assignment of all TMs and reveals principles of subunit packing. Our results also suggest that different detergents, as exemplified by amphipols and digitonin, may have little impact on the core conformation of γ-secretase.

Author contributions: L.S., L.Z., G.Y., C.Y., R.Z., X.Z., T.X., Y.Z., S.W., X.L., and Y.S. designed research; L.S., L.Z., G.Y., C.Y., R.Z., X.Z., and Y.Z. performed research; L.S., L.Z., G.Y., C.Y., R.Z., X.Z., T.X., Y.Z., S.W., X.L., and Y.S. contributed new reagents/analytic tools; L.S., L.Z., G.Y., C.Y., R.Z., X.Z., T.X., Y.Z., S.W., X.L., and Y.S. analyzed data; and Y.S. wrote the paper.

Reviewers: H.L., Stony Brook University; and G.Y., University of Texas Southwestern Medical Center.

The authors declare no conflict of interest.

Freely available online through the PNAS open access option.

Data deposition: The atomic coordinates have been deposited in the Protein Data Bank, www.pdb.org (PDB ID code 4UIS), and the EM maps have been deposited in the Electron Microscopy Data Bank, www.ebi.ac.uk/pdbe/emdb (accession no. EMD-2974).

[1]L.S., L.Z., G.Y., C.Y., and R.Z. contributed equally to this work.

[2]To whom correspondence should be addressed. Email: shi-lab@tsinghua.edu.cn.

This article contains supporting information online at www.pnas.org/lookup/suppl/doi:10.1073/pnas.1506242112/-/DCSupplemental.

Results

Structure Determination of Human γ-Secretase. Although the overall resolution limit for our previous cryo-EM structure of γ-secretase is 4.5 Å, the actual resolution in the TM region is considerably lower and reveals few features for the helices (31). To help identify the TMs in PS1, we fused T4 lysozyme to the amino terminus of PS1, hoping that this design may allow conclusive identification of PS1-TM1 even at a moderate resolution. To investigate the role of detergent on the integrity of γ-secretase, we replaced amphipols by digitonin. The resulting human γ-secretase exhibited excellent solution behavior (Fig. S1*A*) and robust protease activities toward the substrate APP C99 (Fig. S1 *B* and *C*). We imaged the γ-secretase with a K2 direct electron detector mounted on a Titan Krios electron microscope operating at 300 kV (Fig. 1).

In total, 575,155 particles were selected from 3,312 micrographs for reference-free two-dimensional (2D) classification and subsequent three-dimensional (3D) classification (Fig. 1 *A* and *B*). After a second round of 3D classification, 177,207 particles from six classes were subjected to further autorefinement. The final EM density has an overall resolution of 4.32 Å on the basis of the gold standard Fourier Shell Correlation (FSC) criteria (Fig. 1 *C* and *D*). Nineteen TMs display unambiguous α-helical conformation, some with side-chain features (Fig. 2*A* and Figs. S2 and S3).

The central task—identification of PS1—was greatly facilitated by the presence of T4 lysozyme, which is attached to PS1-TM1 on the cytoplasmic side (Fig. 2*A*). The assignment of PS1-TM1, along with the predicted structural homology between PS1 and PSH, allows convenient identification of the other TMs (Fig. S2 *A* and *B*). Notably, PS1-TM2 has little density and belongs to the 20th TM beyond the 19 clearly observed TMs. Based on its connectivity to the ECD, the only TM in nicastrin was unambiguously assigned (Fig. S2 *A* and *C*). The seven TMs, located between nicastrin and PS1, were assigned to Aph-1 (Fig. S2 *A* and *D*). Finally, the remaining three TMs on the thin end of the TM horseshoe were attributed to Pen-2 (Fig. S2 *A* and *E*). The limited resolution only allowed interpretation of the TMs as a poly-Ala model. Importantly, however, the sequence homology between PS1 and PSH was used to generate a candidate atomic model for PS1.

Assembly of γ-Secretase from Four Components. The extracellular region of human γ-secretase is mostly composed of nicastrin ECD, which sits on top of the horseshoe-shaped transmembrane region, making close contacts to the two ends of the TM horseshoe (Fig. 2*B* and Fig. S4). At the thin end, an α-helix and its surrounding structural elements in nicastrin interact with the extracellular portion of Pen-2. At the thick end, the lone TM from nicastrin stacks against TM1/TM5/TM7 of Aph-1 within the lipid membrane, whereas the amino terminus of nicastrin and the β-strand preceding TM associate with the extracellular element of Aph-1 (Fig. 2*B* and Fig. S4).

In contrast to previous prediction (13, 32), Pen-2 contains three TMs, two of which traverse the membrane only half-way from the intracellular side (Fig. 2*B*). Consequently, the amino terminus of Pen-2 is located on the extracellular side and the carboxyl terminus on the cytoplasmic side. TM1 and TM3 from Pen-2 closely pack against TM4 of PS1 (Fig. 2*B* and Fig. S5 *A* and *B*), consistent with results of biochemical characterization (20, 21). The core of the TM horseshoe comprises PS1 and Aph-1, which together contribute 16 TMs. TM8 and TM9 from PS1 form an extensive interface with TM2 and TM4 of Aph-1, with the carboxyl terminus of PS1 inserted into a cavity formed by TMs 2–6 of Aph-1 (Fig. 2*B* and Fig. S5 *A*, *C*, and *D*).

Unexpectedly, TM6 and TM7 of PS1, which harbor the two catalytic residues Asp257 and Asp385, are located on the convex side of the TM horseshoe (Fig. 2*B*). The TM organization and the predicted location of catalytic residues strongly suggest that substrate proteins may gain access to the active site laterally from the convex side of the TM horseshoe. Among the nine TMs of PS1, TM2 has little EM density (Fig. S5*A*), suggesting a high degree of conformational flexibility. Intriguingly, TM2 is located close to TM6, which is also quite flexible as judged by its relatively poor EM density compared with the other TMs in PS1. We speculate that TM2 and TM6 may play a critical role in the regulation of substrate entry and cleavage.

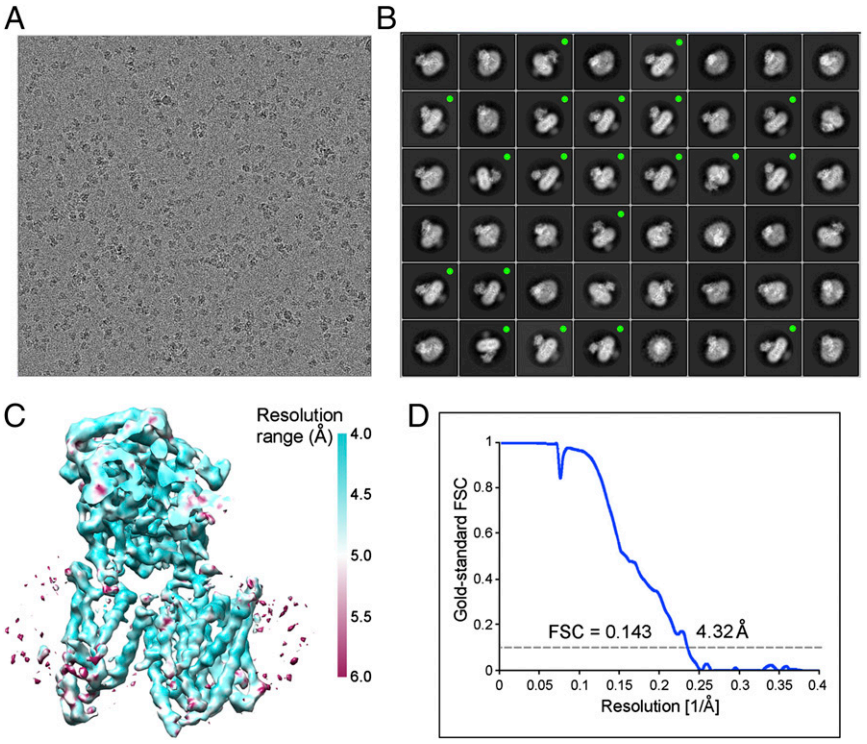

Fig. 1. Cryo-EM analysis of human γ-secretase. (*A*) A representative micrograph of the γ-secretase sample. An entire micrograph is shown. (*B*) Representative 2D classifications of the γ-secretase particle. The duck-shaped side views (identified by green dots) clearly reveal the position of the ECD (large head) and T4 lysozyme (small feet). The majority of the large duck body is formed by the nonspecifically bound detergents, whose contributions are gradually diminished at increasingly higher resolutions. (*C*) An overall view of the EM density for γ-secretase. The resolution is color-coded for different regions of γ-secretase. The relatively uniform resolution contrasts our previous study where the TM region has considerably lower resolutions (31). The EM density maps were generated in Chimera (46). (*D*) The overall resolution is estimated to be 4.32 Å on the basis of gold standard FSC criteria of 0.143.

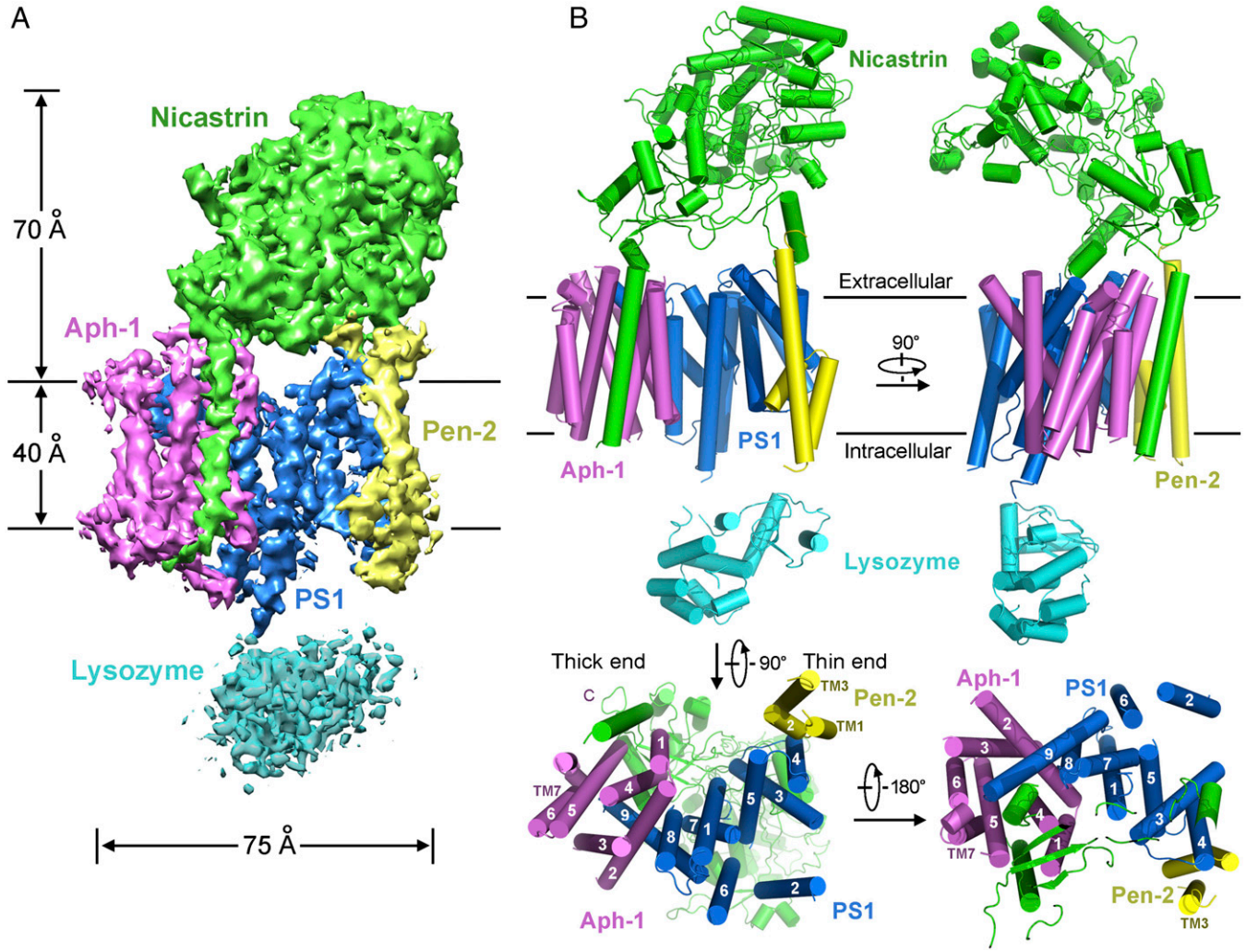

Fig. 2. Overall structure of human γ-secretase. (*A*) An overall view of the EM density at 4.32-Å resolution. Densities for the four components of γ-secretase are color-coded: PS1 (blue), Pen-2 (yellow), Aph-1 (magenta), and nicastrin (green). Except TM2 of PS1, all other 19 TMs display clearly identifiable density. (*B*) Cartoon representation of the γ-secretase structure is shown in four perpendicular views. The four components are color-coded: PS1 (blue), Pen-2 (yellow), Aph-1 (magenta), and nicastrin (green). This coloring scheme is used in the other figures in this article. The 20 TMs assemble into a horseshoe-shaped structure. Notably, TM6 and TM7 of PS1, which harbor the two catalytic residues Asp257 and Asp385, are located on the convex side of the TM horseshoe. The structure figures were prepared using PYMOL (50).

Structure of Presenilin. PS1, the central component of γ-secretase, contains nine TMs that are arranged into a loosely organized structure (Fig. 3*A*). Notably, none of the nine TMs is perpendicular to the lipid membrane, and the loose organization of PS1 appears to be caused, at least in part, by the large tilting angles of the TMs. TM5 from the NTF and TM7 from the CTF, at about 25–35° away from the membrane normal, are located in the center of PS1. TM5 and TM7 directly stack against each other and are surrounded by the other seven tilting TMs. Close examination of PS1 unexpectedly revealed two structural repeats: TMs 3–5 are topologically identical to TMs 7–9. TMs 3–5 can be brought to an approximate alignment with TMs 7–9 through a lateral translation of about 20 Å within the lipid membrane and a clockwise rotation of about 60° around the membrane normal from the extracellular side.

PS1 shares 19% sequence identity and 53% sequence similarity with the archaeal intramembrane protease PSH (29); PS1 and PSH exhibit a similar overall structure (Fig. 3*B*). PS1 and PSH can be aligned to each other with a root-mean-squared deviation (rmsd) of 2.4 Å over 241 aligned Cα atoms. In contrast to many other membrane proteins and the other three components of γ-secretase, both PS1 and PSH contain large cavities that are formed by the tilting TMs (Fig. 3*B*). Most notably, the loose packing from TM2 and TM6 is predicted to engender empty spaces and holes that traverse the lipid membrane. In cells, these transmembrane cavities are presumably occupied by lipid molecules and thus may influence substrate access and catalysis. Such cavities may also be linked to the reported ion channel activities of presenilin (33).

Structure of Aph-1. The core of Aph-1 comprises TM4 and TM5, which are surrounded by a centrally bent helix TM1 on one side and TM6/TM7 on the other side (Fig. 4*A*). These five TMs are nearly perpendicular to the lipid membrane and closely stack against each other throughout their transmembrane regions. In contrast, TM2 and TM3 are tilted at steep angles of 20–40 degrees relative to the membrane normal (Fig. 4*A*). Consequently, TM2 and TM3 are largely separated from the other five TMs on the extracellular side, forming a V-shaped cavity. This cavity serves as the binding site for the carboxyl terminus of PS1 (Fig. S5 *A*, *C*, and *D*).

The seven TMs of Aph-1 appear to adopt a previously unreported membrane protein fold. Exhaustive search of the Protein Data Bank (PDB) by the distance alignment matrix method (DALI) (34) led only to identification of many entries that are homologous to select

BIOCHEMISTRY

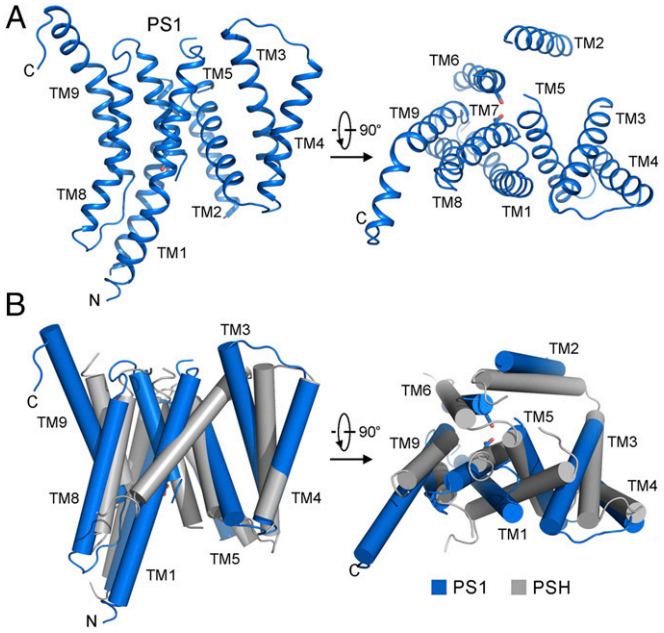

Fig. 3. Structural features of PS1. (*A*) PS1 exhibits a loosely organized structure. PS1 is shown in two perpendicular cartoon representations. The nine TMs are organized into an extended structure, with TM3 and TM4 somewhat distanced from the rest. TM2 lacks EM density. An atomic model for PS1 was built on the basis of sequence and structural homology between PS1 and PSH (29). Predicted positions of the two catalytic residues Asp257 and Asp385 are indicated. (*B*) PS1 is a close structural homolog of PSH. Shown here is an overlay of PS1 (blue) and PSH (gray).

TMs of Aph-1, but not to its entire length. Phenylalanine ammonia lyase (PDB code 1T6P, chain F) (35) exhibits the highest Z-score (similarity score) of 6.9 and can be aligned to TM1 and TMs 4–7 of Aph-1 with an rmsd of 5.3 Å over 139 aligned Cα atoms (Fig. 4*B*, *Left*). On the other hand, a representative protein pyrophosphatase (PDB code 4A01, chain A) (36) has a Z-score of 5.3 and can be aligned to TMs 1–5 of Aph-1 with an rmsd of 5.3 Å over 185 aligned Cα atoms (Fig. 4*B*, *Right*).

Impact of Detergents on γ-Secretase Structure. In our previous study (31), the wild-type human γ-secretase was prepared in amphipols. In the current study, the human γ-secretase, with a T4 lysozyme fused to the amino terminus of PS1, was prepared in the widely used detergent digitonin. Despite these differences, the overall shape and general features of γ-secretase are very similar between these two structures (Fig. 5 *A* and *B*), with their ECDs nearly indistinguishable from each other (Fig. 5*C*). Closer examination of the intramembrane region reveals minor shifts of TMs that are located at the periphery of the TM region (Fig. 5*D*). For example, TM6 in PS1 undergoes a lateral translation of about 5 Å to move closer to the other TMs in the current structure. TM3 and TM4 in PS1 and TMs 1–3 in Pen-2 also exhibit small degrees of lateral shifts (Fig. 5*D*). Nonetheless, the bulk of the TM region remains nearly identical between these two structures of γ-secretase obtained under different detergent conditions.

Discussion

In this study, we report the cryo-EM structure of human γ-secretase at an overall resolution of 4.32 Å. The resolution range is relatively uniform throughout the ECD and the TM regions (Fig. 1*C*). In contrast, our previous cryo-EM resolution of 4.5 Å applies mostly to the ECD, whereas the TM region had a resolution range only of 5–7 Å. Therefore, although the current overall resolution is only 0.2 Å better than before, the fine features in the TM region have shown significant improvement. The improved density in the TMs, together with identification of PS1-TM1 through T4 lysozyme fusion, allows specific assignment of all TMs in human γ-secretase to its four components.

We predicted two possible TM assignments, with PS1 located either at the thick end or at the thin end of the TM horseshoe (31). The latter prediction was supported by the crystal structure of a eukaryotic nicastrin homolog (30), which places its lone TM at the thick end and thus favors the placement of Aph-1 at the thick end and PS1 at the thin end. Scrutiny of the EM density led to identification of eight TMs that resemble the PSH topology and suggested a speculative model of subunit assembly in γ-secretase (30). Our current study confirms this model and reveals additional insights. The previously unknown topology of the seven TMs in Aph-1 is different from that of GPCR (37); the central cavity of Aph-1, which somewhat resembles the ligand-binding pocket of GPCR, embraces the carboxyl terminus of PS1. Gratifyingly, our structure is consistent with a large body of biochemical data on the assembly of γ-secretase (15–21). For example, TM4 of PS1 was shown to bind Pen-2 (20, 21); in our structure, the three TMs of Pen-2 are organized around PS1-TM4.

Pen-2 closely associates with PS1 and presumably depends on PS1 for proper folding. One unanticipated finding is that Pen-2 contains three TMs, not two as previously predicted (13, 32). The previously predicted TM1 consists of a TM hairpin, which goes into the membrane half-way and loops back into the cytoplasm. Consequently, the amino terminus of Pen-2 is located in the cytoplasm but its carboxyl terminus is on the extracellular side. This membrane-spanning topology differs from the previous conclusion that both amino and carboxyl termini of Pen-2 are on the extracellular side (32). The published biochemical data are actually consistent with our structural observation. For example, introduction of a glycosylation site at the carboxyl

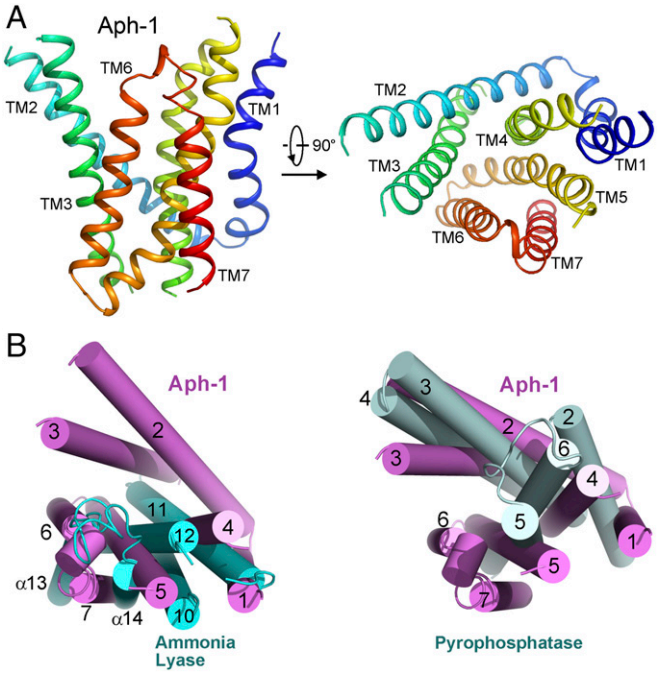

Fig. 4. Structural features of Aph-1. (*A*) Overall structure of Aph-1 is shown in two perpendicular views. The seven TMs are rainbow-colored, with amino terminus in blue and carboxyl terminus in red. (*B*) Structure of Aph-1 may represent a previously unreported membrane protein fold. A DALI (34) search identified two classes of protein that share homology with select regions, but not the entire length, of Aph-1. Shown here are structural comparisons between Aph-1 and phenylalanine ammonia lyase (*Left*, PDB code 1T6P, chain F) (35) or pyrophosphatase (*Right*, PDB code 4A01, chain A) (36).

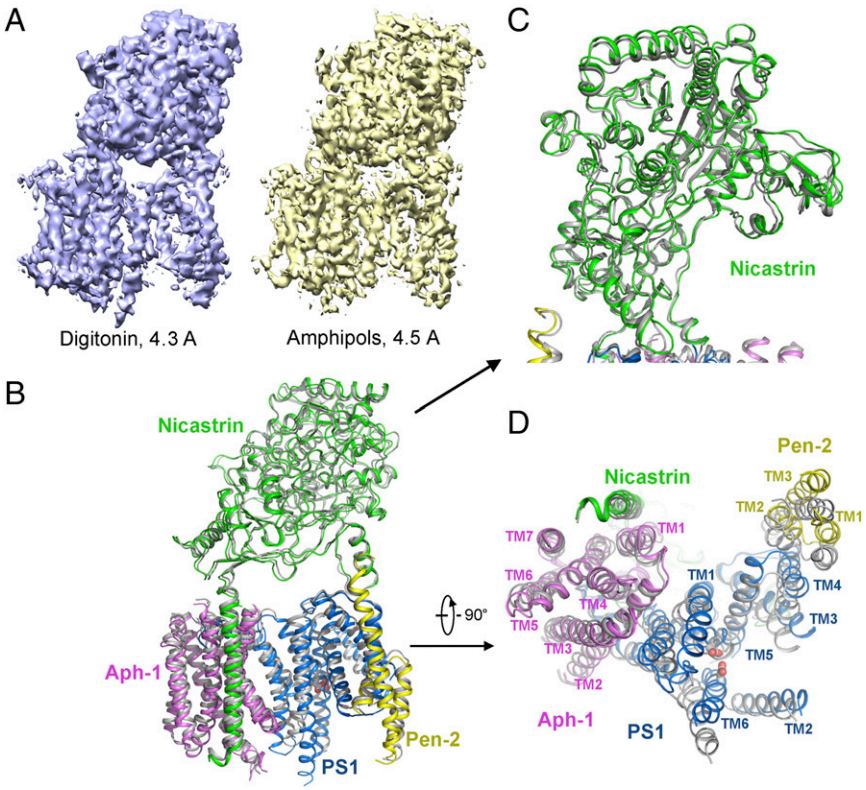

Fig. 5. Impact of detergents on the structure of γ-secretase. (*A*) Comparison of the overall EM densities for γ-secretase under digitonin (*Left*) versus amphipols (*Right*). The fine helical features in the transmembrane region are apparent for the γ-secretase sample under digitonin, but not amphipols. However, the overall shapes of these two structures are nearly identical, ruling out any significant impact by the choice of detergent. (*B*) Comparison of the overall structures of γ-secretase obtained under digitonin (four colors) versus amphipols (gray). (*C*) A close-up comparison of the ECD from the two structures determined under different detergents. (*D*) A close-up comparison of the TM region. A few TMs located at the periphery of the TM horseshoe (TM3/4/6 of PS1 and TMs 1–3 of Pen-2) undergo small degrees of shift.

terminus, but not at the amino terminus, of Pen-2 led to complete glycosylation, whereas the engineered glycosylation site at the amino terminus was barely glycosylated (32).

An important design of this study is the fusion of T4 lysozyme to the amino terminus of PS1, which allows unambiguous assignment of PS1-TM1 and facilitates identification of other TMs. The linker sequence between PS1-TM1 and T4 lysozyme is flexible and unable to fix T4 lysozyme in one orientation relative to γ-secretase. Consequently, the EM density for T4 lysozyme shows well only at lower resolutions. Another important difference from our previous study is the choice of detergent. Because amphipols are viewed as unusual detergents, their use in the EM structure determination raises the concern of potential conformational distortion. Our current study, performed in the frequently used detergent digitonin, reveals an identical overall structure and satisfactorily addresses the concern.

In fact, a prerequisite for structure determination by any biophysical method—pertaining to not just X-ray crystallography or NMR but also cryo-EM—is a stable and homogeneous conformation for a large subset of the target macromolecule. This prerequisite is usually lost under conditions where structure-disturbing molecules such as extremely harsh detergents are profusely used. Thus, any cryo-EM structure that is soundly determined on good samples should represent reality—a stable conformation of the target macromolecule. An argument can be made with regard to whether other conformational states, transient or stable, exist for this macromolecule. However, this argument should in no way affect the validity of the obtained structure.

Our structures differ from other published EM structures of γ-secretase at considerably lower resolutions (22–27). Such differences may be attributed to at least two key factors: sample preparation and image analysis. First, the relatively homogeneous nature of γ-secretase is essential for imaging under microscope. In our experience, such homogeneity should be apparent by the criteria of SDS/PAGE using Coomassie blue staining (not Western blots), gel filtration (to show the monodisperse nature), and cryo-EM conditions (to ensure particle intactness under frozen condition). Second, caution and technically sound practice must be exercised in image acquisition and analysis and structure determination. In the case of γ-secretase, at low resolutions, the thick shell of detergents that surround the TM region gives rise to the appearance of a duck body whereas the ECD resembles the head (Fig. 1*B*). This general feature has been observed in our investigation (Fig. 1*B*) and other studies (26, 27, 31). Only at higher resolutions can the influence from the nonspecifically bound detergents (which thus lack order) be removed.

In summary, the cryo-EM structure of γ-secretase at 4.3-Å resolution reveals principles of γ-secretase assembly from its four subunits and serves as an important reference for future structural and functional investigation of γ-secretase.

Materials and Methods

Protein Preparation. The amino-terminal 75 residues in PS1 are flexible and exhibit little EM density (31). The predicted PS1-TM1 begins at residue 78. The cDNA for T4 lysozyme was placed at the 5′-end of the DNA sequence encoding residues 69–467 of PS1, using the pMLink vector (31). The other three components were the same as previously reported (31). Culture and transfection of HEK 293S GnTI$^-$ cells [American Type Culture Collection (ATCC)] and purification of γ-secretase were as described (31), except that amphipols were replaced by 0.1% digitonin (Sigma). In the last step, the purified γ-secretase was fractionated on a Superose-6 column (GE Healthcare) in 0.1% digitonin, 25 mM Hepes, pH 7.4, and 150 mM NaCl. The peak fractions were concentrated for cryo-EM grid preparation or were used for activity assays.

Activity Assays. Purified wild-type or T4 lysozyme fused γ-secretase, either in amphipols or digitonin, was mixed with APP-C99 in 0.2% 3-[(3-cholamidopropyl)dimethylammonio]-2-hydroxy-1-propanesulfonate (CHAPSO), 50 mM Hepes, pH 7.0, 0.1% phosphatidylcholine, and 0.025% phosphatidylethanolamine and incubated at 37 °C for 4 h as described (38). To detect the cleavage products Aβ40 and Aβ42, the AlphaLISA assay was performed following the standard protocol as described in the AlphaLISA kit (PerkinElmer). Briefly, 2-μL reaction samples were incubated at 22 °C for 1 h with 8 μL AlphaLISA Aβ1–40/42 Acceptor beads. After a 30-min incubation with 10 μL AlphaLISA Aβ1–40/42 donor beads in darkness at 22 °C, the samples were read by an Envision-Alpha Reader (PerkinElmer). The assay was repeated at least three times for each data point.

Cryo-EM Data Acquisition. Cryo-EM grids were prepared with Vitrobot Mark IV (FEI). Aliquots of 3 μL T4-lysozyme fused γ-secretase at 25 μM were applied to glow-discharged Quantifoil Cu R1.2/1.3 grids, blotted for 4 s, and plunged into liquid ethane cooled by liquid nitrogen. The samples were imaged by Titan Krios (FEI) at 300 kV with a nominal magnification of 22,500. Defocus varied from 1.3 to 3.0 μm. Images were recorded by a K2 Summit counting camera (Gatan Company) with superresolution mode and binned to a pixel size of 1.32 Å. Each image was dose-fractionated to 32 frames with a dose rate of ∼6 counts per second per physical pixel (∼4.5 e^-/s $Å^2$), a total exposure time of 10.4 s, and 0.325 s per frame. UCSFImage4 was used for all data collection (developed by X.L.).

Image Processing. The images were aligned and summed using the whole-image motion correction (39). The defocus value of each image was determined by CTFFIND3 (40). A total of 575,155 particles were picked from 3,312 micrographs using the automatic particle picking subroutine in RELION (41). Using RELION and IMAGIC (42), a reference-free 2D classification was performed, yielding 409,909 good particles. The initial 3D model for further 3D analysis was generated using EMAN2 subroutine e2initialmodel.py (43). Similar to our previous work (31), the initial model has an overall duck-like shape. The handedness of the initial model was determined and corrected by the comparison. Three-dimensional classification and refinement were carried out using RELION 1.3 (41). Through 3D classification against the initial model low-pass–filtered to 60 Å, 409,909 particles were classified to generate the most homogeneous class of 219,144 particles. The autorefine procedure of this class produced a 3D reconstruction with a resolution of 4.47 Å, which showed clear secondary structural elements. Using the 219,144 particles, we performed a second-round of 3D classification against the 4.47 Å model, with an eight-class designation and 3.7° precision for local angular search. A total of 177,207 particles from the best six classes were selected for further autorefining. The final 3D reconstruction shows an overall resolution of 4.32 Å based on the gold standard FSC corrected by the phase randomization approach (44). The final density maps were sharpened by applying a negative B-factor estimated by automated procedures. Local resolution was estimated using ResMap (45).

Model Building and Refinement. The atomic models for nicastrin ECD and PS1 were generated from the crystal structures of DpNCT (PDB ID: 4R12) (30) and PSH (PDB ID: 4HYG) (29) by CHAINSAW (46) and docked into the density map by CHIMERA (47). T4 lysozyme was fitted into the density map manually by COOT (PDB ID: 4S0W). Poly-Ala models for the TMs of Aph-1, Pen-2, and nicastrin were manually built by COOT (48). The structure was refined in real space by PHENIX (49) with secondary structure restraint and manually adjusted in COOT.

ACKNOWLEDGMENTS. We thank Hongwei Wang for discussion, and Jiao Lin and Guangwen Yang for assistance at the Explorer 100 cluster system of Tsinghua National Laboratory for Information Science and Technology. This work was supported by funds from the Ministry of Science and Technology (2014ZX09507003006) and the National Natural Science Foundation of China (31130002 and 31321062).

1. De Strooper B, Iwatsubo T, Wolfe MS (2012) Presenilins and gamma-secretase: Structure, function, and role in Alzheimer disease. *Cold Spring Harbor Perspect Med* 2(1):a006304.
2. Goate A, Hardy J (2012) Twenty years of Alzheimer's disease-causing mutations. *J Neurochem* 120(Suppl 1):3–8.
3. De Strooper B, et al. (1998) Deficiency of presenilin-1 inhibits the normal cleavage of amyloid precursor protein. *Nature* 391(6665):387–390.
4. Selkoe DJ, Wolfe MS (2007) Presenilin: Running with scissors in the membrane. *Cell* 131(2):215–221.
5. Morishima-Kawashima M (2014) Molecular mechanism of the intramembrane cleavage of the β-carboxyl terminal fragment of amyloid precursor protein by γ-secretase. *Front Physiol* 5:463.
6. Hardy JA, Higgins GA (1992) Alzheimer's disease: The amyloid cascade hypothesis. *Science* 256(5054):184–185.
7. Thinakaran G, et al. (1996) Endoproteolysis of presenilin 1 and accumulation of processed derivatives in vivo. *Neuron* 17(1):181–190.
8. Wolfe MS, et al. (1999) Two transmembrane aspartates in presenilin-1 required for presenilin endoproteolysis and gamma-secretase activity. *Nature* 398(6727):513–517.
9. Shah S, et al. (2005) Nicastrin functions as a gamma-secretase-substrate receptor. *Cell* 122(3):435–447.
10. Dries DR, et al. (2009) Glu-333 of nicastrin directly participates in gamma-secretase activity. *J Biol Chem* 284(43):29714–29724.
11. Goo JS, et al. (2013) Nicastrin overexpression in transgenic mice induces aberrant behavior and APP processing. *Mol Neurobiol* 48(1):232–243.
12. Takasugi N, et al. (2003) The role of presenilin cofactors in the gamma-secretase complex. *Nature* 422(6930):438–441.
13. Francis R, et al. (2002) aph-1 and pen-2 are required for Notch pathway signaling, gamma-secretase cleavage of betaAPP, and presenilin protein accumulation. *Dev Cell* 3(1):85–97.
14. Goutte C, Tsunozaki M, Hale VA, Priess JR (2002) APH-1 is a multipass membrane protein essential for the Notch signaling pathway in Caenorhabditis elegans embryos. *Proc Natl Acad Sci USA* 99(2):775–779.
15. Gu Y, et al. (2003) APH-1 interacts with mature and immature forms of presenilins and nicastrin and may play a role in maturation of presenilin.nicastrin complexes. *J Biol Chem* 278(9):7374–7380.
16. LaVoie MJ, et al. (2003) Assembly of the gamma-secretase complex involves early formation of an intermediate subcomplex of Aph-1 and nicastrin. *J Biol Chem* 278(39):37213–37222.
17. Steiner H, Winkler E, Haass C (2008) Chemical cross-linking provides a model of the gamma-secretase complex subunit architecture and evidence for close proximity of the C-terminal fragment of presenilin with APH-1. *J Biol Chem* 283(50):34677–34686.
18. Kaether C, et al. (2004) The presenilin C-terminus is required for ER-retention, nicastrin-binding and gamma-secretase activity. *EMBO J* 23(24):4738–4748.
19. Fraering PC, et al. (2004) Detergent-dependent dissociation of active gamma-secretase reveals an interaction between Pen-2 and PS1-NTF and offers a model for subunit organization within the complex. *Biochemistry* 43(2):323–333.
20. Kim SH, Sisodia SS (2005) Evidence that the "NF" motif in transmembrane domain 4 of presenilin 1 is critical for binding with PEN-2. *J Biol Chem* 280(51):41953–41966.
21. Watanabe N, et al. (2005) Pen-2 is incorporated into the gamma-secretase complex through binding to transmembrane domain 4 of presenilin 1. *J Biol Chem* 280(51):41967–41975.
22. Lazarov VK, et al. (2006) Electron microscopic structure of purified, active gamma-secretase reveals an aqueous intramembrane chamber and two pores. *Proc Natl Acad Sci USA* 103(18):6889–6894.
23. Ogura T, et al. (2006) Three-dimensional structure of the gamma-secretase complex. *Biochem Biophys Res Commun* 343(2):525–534. and erratum (2006) 345(1):543.
24. Osenkowski P, et al. (2009) Cryoelectron microscopy structure of purified gamma-secretase at 12 A resolution. *J Mol Biol* 385(2):642–652.
25. Renzi F, et al. (2011) Structure of gamma-secretase and its trimeric pre-activation intermediate by single-particle electron microscopy. *J Biol Chem* 286(24):21440–21449.
26. Li Y, et al. (2014) Structural interactions between inhibitor and substrate docking sites give insight into mechanisms of human PS1 complexes. *Structure* 22(1):125–135.
27. Elad N, et al. (2014) The dynamic conformational landscape of γ-secretase. *J Cell Sci* 128(3):589–598.
28. Sobhanifar S, et al. (2010) Structural investigation of the C-terminal catalytic fragment of presenilin 1. *Proc Natl Acad Sci USA* 107(21):9644–9649.
29. Li X, et al. (2013) Structure of a presenilin family intramembrane aspartate protease. *Nature* 493(7430):56–61.
30. Xie T, et al. (2014) Crystal structure of the γ-secretase component nicastrin. *Proc Natl Acad Sci USA* 111(37):13349–13354.
31. Lu P, et al. (2014) Three-dimensional structure of human γ-secretase. *Nature* 512(7513):166–170.
32. Crystal AS, et al. (2003) Membrane topology of gamma-secretase component PEN-2. *J Biol Chem* 278(22):20117–20123.
33. Tu H, et al. (2006) Presenilins form ER Ca2+ leak channels, a function disrupted by familial Alzheimer's disease-linked mutations. *Cell* 126(5):981–993.
34. Holm L, Sander C (1993) Protein structure comparison by alignment of distance matrices. *J Mol Biol* 233(1):123–138.
35. Calabrese JC, Jordan DB, Boodhoo A, Sariaslani S, Vannelli T (2004) Crystal structure of phenylalanine ammonia lyase: Multiple helix dipoles implicated in catalysis. *Biochemistry* 43(36):11403–11416.
36. Lin SM, et al. (2012) Crystal structure of a membrane-embedded H+-translocating pyrophosphatase. *Nature* 484(7394):399–403.
37. Rasmussen SG, et al. (2007) Crystal structure of the human beta2 adrenergic G-protein-coupled receptor. *Nature* 450(7168):383–387.
38. Dang S, et al. (2015) Cleavage of amyloid precursor protein by an archaeal presenilin homologue PSH. *Proc Natl Acad Sci USA* 112(11):3344–3349.
39. Li X, et al. (2013) Electron counting and beam-induced motion correction enable near-atomic-resolution single-particle cryo-EM. *Nat Methods* 10(6):584–590.
40. Mindell JA, Grigorieff N (2003) Accurate determination of local defocus and specimen tilt in electron microscopy. *J Struct Biol* 142(3):334–347.
41. Scheres SH (2012) RELION: Implementation of a Bayesian approach to cryo-EM structure determination. *J Struct Biol* 180(3):519–530.
42. van Heel M, Harauz G, Orlova EV, Schmidt R, Schatz M (1996) A new generation of the IMAGIC image processing system. *J Struct Biol* 116(1):17–24.
43. Tang G, et al. (2007) EMAN2: An extensible image processing suite for electron microscopy. *J Struct Biol* 157(1):38–46.
44. Chen S, et al. (2013) High-resolution noise substitution to measure overfitting and validate resolution in 3D structure determination by single particle electron cryomicroscopy. *Ultramicroscopy* 135:24–35.
45. Kucukelbir A, Sigworth FJ, Tagare HD (2014) Quantifying the local resolution of cryo-EM density maps. *Nat Methods* 11(1):63–65.
46. Stein N (2008) CHAINSAW: A program for mutating pdb files used as templates in molecular replacement. *J Appl Crystallogr* 41:641–643.
47. Pettersen EF, et al. (2004) UCSF Chimera: A visualization system for exploratory research and analysis. *J Comput Chem* 25(13):1605–1612.
48. Emsley P, Cowtan K (2004) Coot: Model-building tools for molecular graphics. *Acta Crystallogr D Biol Crystallogr* 60(Pt 12 Pt 1):2126–2132.
49. Adams PD, et al. (2010) PHENIX: A comprehensive Python-based system for macromolecular structure solution. *Acta Crystallogr D Biol Crystallogr* 66(Pt 2):213–221.
50. DeLano WL (2002) The PyMOL Molecular Graphics System. Available at www.pymol.org. Accessed April 16, 2015.